TOPICAL REVIEW — Magnetism, magnetic materials, and interdisciplinary research

Multifunctional magnetic nanoparticles for magnetic resonance image-guided photothermal therapy for cancer*

Yue Xiu-Li(岳秀丽)[a], Ma Fang(马 放)[a], Dai Zhi-Fei(戴志飞)[b]†

[a] State Key Laboratory of Urban Water Resources and Environment, School of Municipal and Environmental Engineering, Harbin Institute of Technology, Harbin 150001, China

[b] Department of Biomedical Engineering, College of Engineering, Peking University, Beijing 100871, China

(Received 12 October 2013; revised manuscript received 6 November 2013; published online 20 March 2014)

Key advances in multifunctional magnetic nanoparticles (MNPs) for magnetic resonance (MR) image-guided photothermal therapy of cancer are reviewed. We briefly outline the design and fabrication of such multifunctional MNPs. Bimodal image-guided photothermal therapies (MR/fluorescence and MR/ultrasound) are also discussed.

Keywords: magnetic nanoparticles, magnetic resonance imaging, fluorescence imaging, ultrasound imaging, photothermal therapy

PACS: 43.25.+y, 43.35.+d, 85.70.Ec **DOI:** 10.1088/1674-1056/23/4/044301

1. Introduction

Due to the ease of manipulating and controlling magnetic nanoparticles (MNPs) by an external magnetic field, they are employed in sophisticated ways such as in magnetically targeting drug delivery, and in improving therapies' efficacy and minimizing their side effects. Of particular note, MNPs have been used clinically as a magnetic resonance imaging (MRI) contrast agent. Image-guided photothermal therapy (PTT) has drawn extensive research interest, owing to its minimal invasiveness. Multifunctional MNPs with the combination of MRI and PTT would be of great value to obtain more comprehensive diagnostic information, particularly the dynamics of disease progression, for the accurate location of a therapeutic focusing spot in the targeted tumor tissue. So cancer PTT with near-infrared (NIR) light and photoabsorbers has attracted wide research interest due to its minimal invasiveness compared with other cancer interventions that unavoidably damage or excise healthy cells along with cancerous cells, such as chemotherapy, radiation therapy, and surgery.[1–3] Nonetheless, before PTT, it is necessary to accurately identify the location and size of tumors as well as the presence of photoabsorbers for laser irradiation.[4–6] In addition, during therapy we need to monitor the treatment procedure in real time to ensure complete eradication of microscopic tumors. Moreover, after therapy we should assess its effectiveness. All these tasks could be carried out by the integration of contrast-enhanced diagnostic imaging capability with photothermal therapy.[7–10]

Image-guided therapy employed diagnostic imaging modalities for planning, targeting, monitoring, controlling and assessing treatment response during the therapeutic treatment.[11–16] As one of the most exciting and challenging strategies for cancer treatment, image-guided tumor ablation has been widely used in both biomedical research and clinical trials.[17–20] Due to the great repercussions of multifunctional nanoparticles (NPs) on clinical diagnosis and therapeutic protocol, their development for both imaging and therapy is pursued with increasing zeal.[21] The administration of multiple doses of theranostic agents commonly adds stress on the body's blood-clearance mechanisms, and NP-based agents could avoid this.[20]

Magnetic NPs have been applied in both biomedical research and clinical trials and turn out to be one of the most promising nanomaterials for both diagnostic and therapeutic agents.[22–26] Superparamagnetic iron oxide nanoparticles (SPIOs) were the first nanoparticulate MRI contrast agent to be used clinically.[27–29] Due to their ease of manipulation and control using an external magnetic field, SPIO NPs are also employed in sophisticated magnetically targeted drug-delivery systems for regulating drug release, and in improving therapies' efficacy and minimizing their side effects.[22–26] In addition, various functional components can be attached to magnetic NPs. Such multifunctional MNPs bear therapeutic moieties, as well as complementary imaging moieties for the investigation of the particle localization across a number of platforms, such as magnetic resonance, optical, or nuclear imaging.[27–29] The present review will briefly outline the design and fabrication of multifunctional MNPs for image-guided photothermal therapy of cancer.

*Project supported by the National Natural Science Foundation of China (Grant Nos. 81371580 and 21273014), the State Key Program of the National Natural Science Foundation of China (Grant No. 81230036), and the National Natural Science Foundation for Distinguished Young Scholars (Grant No. 81225011).

†Corresponding author. E-mail: zhifei.dai@pku.edu.cn; Homepage: http://bme.pku.edu.cn/ daizhifei

© 2014 Chinese Physical Society and IOP Publishing Ltd

2. ICG-loaded MNPs for MR/fluorescence bimodal image-guided PTT

2.1. Fabrication of ICG-loaded SPIO NPs

The NIR fluorescence probe allows deeper penetration of tissues than visible optical probes for *in vivo* imaging applications, leading to 1) high sensitivity, 2) relatively low tissue absorption, and 3) minimal autofluorescence.[30–32] But fluorescent imaging's strong light-scattering unfortunately limits its spatial resolution in turbid media (e.g. tissues). When MRI is used, no such scattering occurs. Indocyanine green (ICG), with absorption and emission maxima in the NIR region around 740 nm and 800 nm, has been approved by the U.S. Food and Drug Administration (FDA) for human medical imaging and diagnosis in clinical applications.[33,34] However, several major challenges remain in the use of ICG for imaging applications, such as temperature- and light-dependent optical properties, a tendency to aggregate and degrade rapidly in aqueous solution, rapid clearance from the body with a short half-life of 2 min–4 min, a tendency toward photobleaching and imprecise targeting. So the indocyanine green cannot be utilized for sensitive and prolonged imaging *in vivo*.[35] In order to resolve these problems, a nanotheranostic agent was developed by coating oleylamine-stabilized SPIO NPs with 1,2-distearoyl-sn-glycero-3-phosphoethanolamine-N-[methoxy (polyethylene glycol)-5000] (DSPE-PEG5000), through a dual solvent exchange method, followed by loading ICG molecules into the lipid layer on the surface of the NPs for photothermal tumor ablation under the guidance of fluorescence/MR bimodal imaging (Fig. 1).[36] Before and after ICG loading, the SPIO NPs were well-dispersed in water with an average hydrodynamic diameter of 29.9 nm and 27.5 nm, respectively. Introduction of the PEG layer on the surface of nanoparticles could greatly prolong the circulation time *in vivo*, thus facilitating biomedical applications of these nanoparticles.

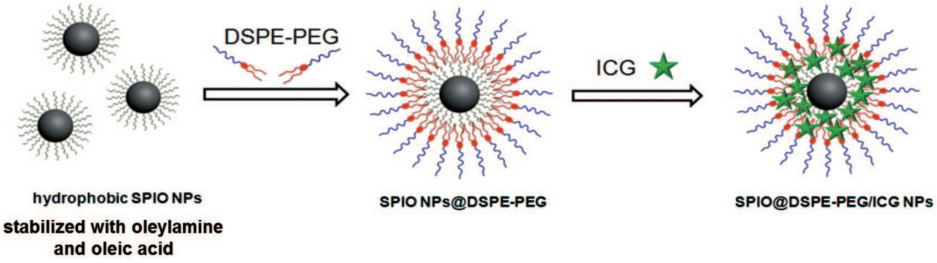


Fig. 1. Schematic illustration of SPIO@DSPE-PEG/ICG NP preparation.[36]

2.2. *In vivo* MR/fluorescence bimodal imaging of ICG-loaded SPIO NPs

Both MRI and fluorescence contrast behavior of the obtained NPs were evaluated *in vitro* and *in vivo*. The magnetic resonance imaging capability of the SPIO@DSPE-PEG/ICG NPs was analyzed *in vivo* using nude mice with grafted tumors (Fig. 2). Twenty four hours after the injection, the whole tumor area became much darker, suggesting that a large number of SPIO@DSPE-PEG/ICG NPs had accumulated in the tumor area, reducing the T_2-weighted MR intensity.

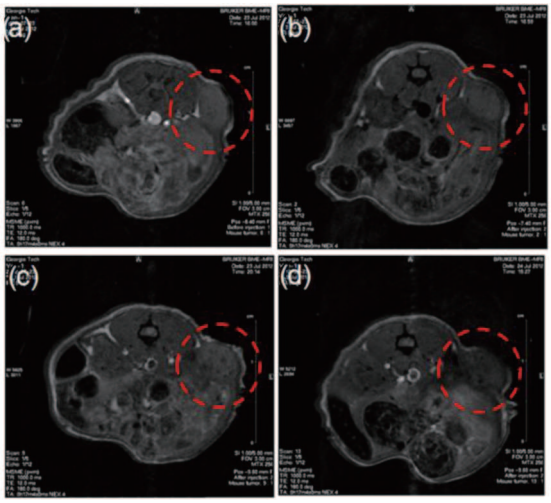


Fig. 2. T_2-weighted MR images of nude mice bearing Hela tumors at (a) 0 h, (b) 0.5 h, (c) 4 h, and (d) 24 h after tail-vein injection of SPIO@DSPE-PEG/ICG NPs.[36]

Twenty four hours after the injection of SPIO@DSPE-PEG/ICG NPs via the tail vein, the fluorescence signals were predominantly located around the tumor, with little from the vital organs, while no intense fluorescence signals were observed throughout the mouse's body at 0.5 h and 4 h after the injection (Fig. 3). In contrast, the free ICG molecules were quickly excreted from the liver within 24 h of injection.[37] These observations suggest that a large number of SPIO@DSPE-PEG/ICG NPs circulated in the blood and then accumulate at the tumor site, which is good evidence of the high efficiency of the tumor-targeting potential of these nanoparticles. Because of the enhanced permeation and retention (EPR) effect, SPIO@DSPE-PEG/ICG NPs of around 30-

nm diameter can be passively accumulated in tumor tissue.[38] In addition, the introduction of the PEG layer on the surface of SPIO NPs inhibits macrophage recognition by the reticuloendothelial system (RES) of the liver and spleen due to the good hydration property, resulting in prolonged circulation in the blood. *In vivo* MR and fluorescence images indicate the high tumor targeting efficiency of SPIO@DSPE-PEG/ICG NPs. The passively targeted SPIO@DSPE-PEG/ICG NPs can also display the tumor area to guide the NIR laser irradiation for photothermal ablation of tumors without damaging the surrounding healthy tissues.

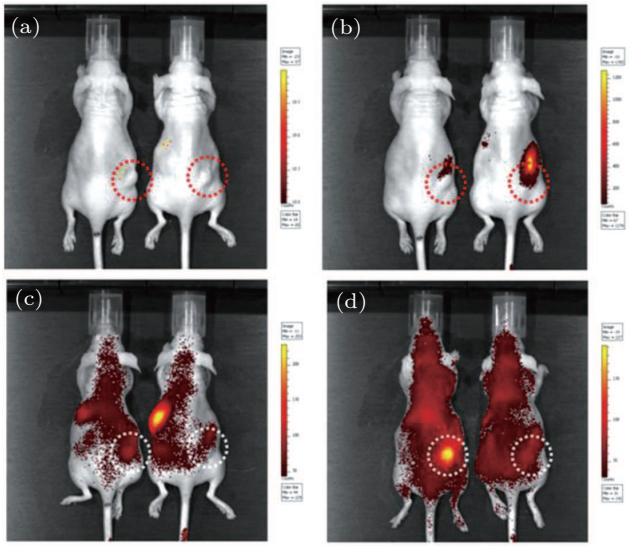


Fig. 3. Fluorescence images of nude mice bearing Hela tumor at (a) 0 h, (b) 0.5 h, (c) 4 h, and (d) 24 h after tail-vein injection of SPIO@DSPE-PEG/ICG NPs (left) and free ICG (right).[36]

2.3. *In vivo* photothermal therapy with ICG-loaded SPIO NPs

The ICG loaded into SPIO NPs significantly improves photostability compared with free ICG and induces intense temperature elevation upon NIR laser irradiation. So, further *in vivo* photothermal therapy was investigated using SPIO@DSPE-PEG/ICG NPs in nude mouse xenograft models. After intravenous injection of SPIO@DSPE-PEG/ICG NPs followed by NIR laser irradiation, the growth of the mice's tumors was first significantly inhibited and then ceased after 14 days of irradiation, while the tumors in saline only, those in saline with laser irradiation and those with SPIO@DSPE-PEG/ICG NPs only all grew significantly over the same time period. These results indicate that neither the NPs nor laser irradiation alone had significant beneficial effect on tumor growth. Tumors were effectively ablated only with the combination of the SPIO@DSPE-PEG/ICG NP injection and NIR laser irradiation, leaving black scars at their original sites with no recurrence (Fig. 4).

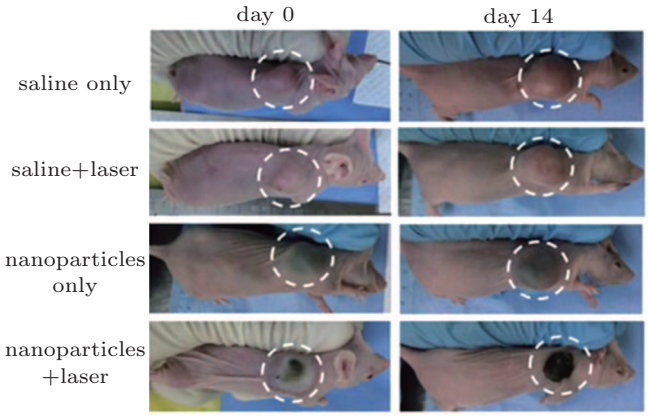


Fig. 4. Representative photographs of mice after *in vivo* photothermal therapy with various treatments, as indicated.[36]

3. Gold-nanoshelled magnetic cerasomes for MRI-guided photothermal therapy

3.1. Cerasomes combine the advantages of both liposomes and silica nanoparticles

Liposomes have been made capable of thermally controlled release of encapsulated agents by forming gold nanoshells on the surface of the liposomes and then controlling the release by heating the gold and hence the liposome membrane above the membrane's melting temperature (T_m) by laser irradiation.[39] A T_m close to body temperature results in drug leakage during circulation in the human system. In contrast, a T_m far above body temperature minimizes leakage during circulation.[40] Due to the insufficient stability of familiar liposomes, gold nanoshell-coated liposomes usually form large gold aggregates, resulting in a one-time release profile instead of multiple-release dynamics.[41]

Recently, a super-stable, freestanding cerasome has been reported as a novel drug delivery system, since its atomic-thick silica-like surface layer imparts a higher morphological stability than can be found in liposomes, and its liposomal bilayer structure reduces the overall rigidity and density greatly, compared to silica nanoparticles.[42–46] Because of the introduction of the liposomal architecture, cerasomes are more biocompatible than silica nanoparticles. Cerasomes possess the advantages of both liposomes and silica nanoparticles but overcome their practical disadvantages, so cerasomes are ideal drug delivery systems.[47] Cholesteryl hemisuccinate (CS) is a cholesterol derivative. Thus, we fabricated gold-nanoshelled magnetic cerasomes (GNMCs) by loading both doxorubicin and Fe_3O_4 MNPs into CS cerasomes and then forming gold nanoshells on the surface of the CS cerasomes (Fig. 5).[48,49]

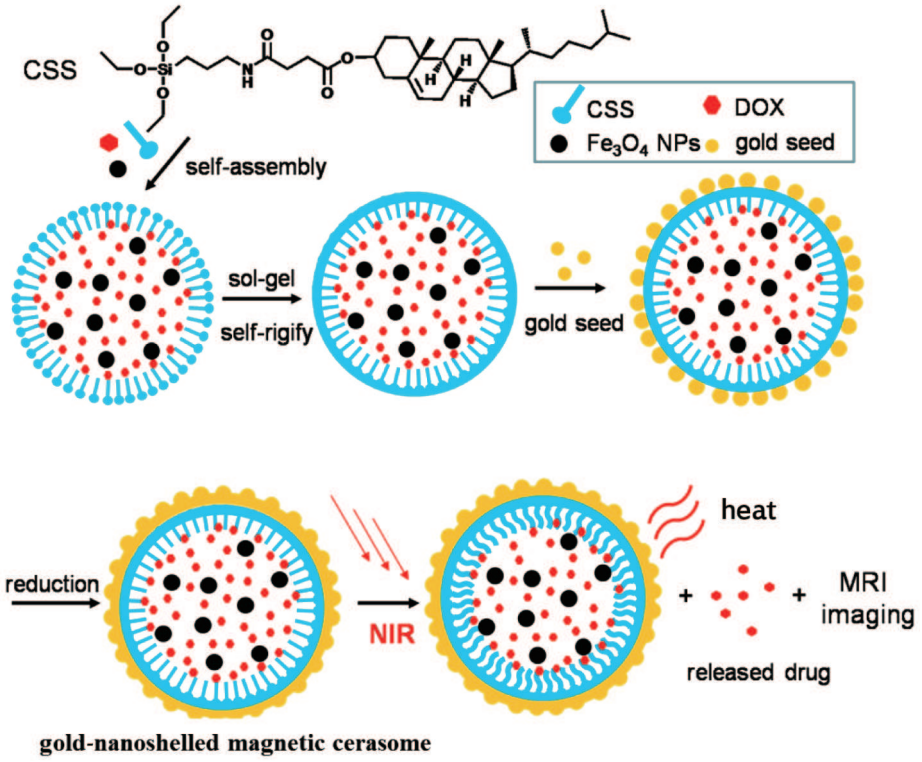


Fig. 5. Schematic illustration of gold-nanoshelled magnetic cerasome.[49]

3.2. Contrast-enhanced MRI imaging using GNMCs

The T_2-enhancing capability of GNMCs with various iron concentrations was compared with that of Fe_3O_4 NPs (with the same iron concentration) by T_2-weighted MRI. The signal intensity of MRI decreased with the increase of iron concentration for both GNMCs and Fe_3O_4 NPs. The weighted transverse relaxivity value (r_2) of the GNMCs was 61.5 mM $Fe^{-1}{\cdot}s^{-1}$, much higher than that of the Fe_3O_4NPs (8.8 mM $Fe^{-1}{\cdot}s^{-1}$). The increase in the transverse relaxivity is attributed to the nanoparticles' assembly into clusters or aggregates in cerasomes, which increases the cross-sectional area.[50,51] This phenomenon offers us an opportunity to identify the location and size of tumors, monitor therapeutic effectiveness and address the drug accumulation in the tumor, all through contrast-enhanced MRI imaging.

3.3. Synergistic effect in killing cancer cells using GNMCs

Superparamagnetism is important in drug delivery. It has been found that homogenously dispersed magnetic cerasomes can be redistributed quickly by external magnetic field and can be redispersed quickly with a slight shake after removal of the magnetic field. A cellular uptake study showed that the concentration of magnetic cerasomes by means of an external magnetic field enables their rapid and efficient uptake by cancer cells, resulting in a higher kill rate for tumor cells than that of drug-loaded nonmagnetic cerasomes.[52] The magnetic field enforces a tight and sustained interaction between the cerasomes and the targeted cell surface to achieve drug delivery. The study's results indicate the suitability of magnetic cerasomes for targeting and separation as drug carriers, and such cerasomes' great potential in anticancer applications.

GNMCs exhibit an NIR-induced temperature elevation and NIR light–triggered, stepwise release of doxorubicin, due to the surface plasmon absorbance in the NIR region and frequency-specific characteristics of CS cerasomes. When GNMCs were exposed to NIR light for 10 min five times, the cumulative amount of DOX released over the whole experimental process was about 2-fold greater than when performed without laser irradiation. Although the amount of DOX released after each irradiation decreased from the first cycle to the fifth cycle, which results from increased coverage of gold nanoshells due to the melting effect of the gold nanostructure,[53] a stepwise triggered release was successfully obtained by NIR irradiation of GNMCs. This multiple-release dynamic can be attributed to the unique characteristics of CS cerasomes — their melting temperature, mechanical stability, and heat resistance are all remarkably higher than those of familiar liposomes, which usually exhibit a one-time release instead of multiple releases.[41] Photothermal cytotoxicity and cell viability *in vitro* tests indicate the feasibility of using GNMCs in photothermal treatment under near-infrared irradiation. A synergistic effect in killing cancer cells might be found by a combination of photothermal therapy, chemotherapy, and magnetic field-guided drug delivery with the aid of

MRI imaging guidance.

4. Gold-nanoshelled magnetic nanocapsules for MR/ultrasound bimodal image-guided photothermal therapy

4.1. SPIOs-embedded PFOB nanocapsules with PEGylated gold shells (PGS-SP NCs)

Compared with other diagnostic imaging modalities, ultrasound (US) imaging has the advantages of real-time, low cost, high safety, and ready availability in portable devices.[54,55] However, the spatial and anatomical resolution of US images has been relatively poor.[56] Nevertheless, these disadvantages of US might be overcome by its integration with MRI.[57] A combination of US and MRI imaging capabilities with PTT could be achieved in a multifunctional theranostic platform. For this purpose, the SPIO-embedded PFOB nanocapsules with PEGylated gold shells were synthesized via an adapted oil-in-water (O/W) emulsion solvent evaporation process, followed by the formation of gold nanoshells using a surface seeding method and surface PEGylation with methoxy-poly(ethylene glycol)-thiol (Fig. 6).[58] Scanning electron micrographs show that PGS-SP NCs keep their spherical shape after gold shell formation but exhibit rough surface morphology,

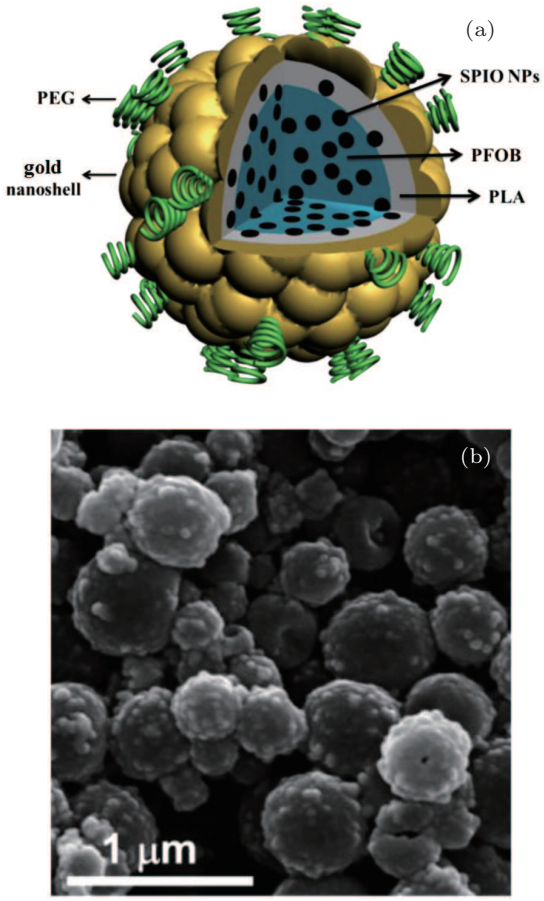


Fig. 6. Schematic illustration (a) and scanning electron micrograph (b) of SPIO-embedded PFOB nanocapsules with PEGylated gold shells.[58]

and their average diameter was about 370 nm. Such a single nanotheranostic agent with the combination of US and MR imaging would be of great value to obtain more comprehensive diagnostic information and probe the dynamics of disease progression for more accurate location of the targeted tumor tissue for more effective PTT tumor ablation.

4.2. Bimodal US/MRI contrast imaging capability of PGS-SP NCs

Bimodal US/MRI contrast image-guided photothermal tumor ablation was performed on nude mouse xenograft models. US imaging guidance was performed under real-time monitoring using a clinical US imaging system (Fig. 7(a)). The tumor was first found and shown in the conventional B-mode, and no ultrasonographic enhancement was observed before injection. Then, the imaging mode was changed to PIHI contrast mode, and in contrast the boundary and size of the tumors can be clearly detected in real-time after the agent injection, suggesting that US imaging can help ensure the complete distribution of the PGS-SP NCs to guide subsequent photoablation therapy.

The PGS-SP NCs also exhibit excellent contrast enhancement, increasing along with the rise of the concentration as shown in the T_2-weighted MR images with high T_2 relaxivity of 395.7±8.0 $mM^{-1}\cdot s^{-1}$, which is more than 2 times as high as that of the commercial SPIO-based MRI contrast agent Resovist (185.8±9.3 $mM^{-1}\cdot s^{-1}$),[59] ensuring good MRI contrast enhancement. The higher T_2 relaxivity is probably due to the aggregation of SPIOs in the nanocapsules, enlarging the magnetic nanoparticles somewhat, which could increase the T_2 relaxivity.[23] When the agent is injected intravenously into the tumor-bearing mice, the nanocapsules tend to accumulate in the tumor sites due to the "enhanced permeability and retention" effect of the nanometer scale and the surface PEGylation of the nanocapsules. The tumor darkened somewhat 0.5 h later, suggesting the SPIO functionalized nanocapsules had been aggregated in the tumor site to generate negative contrast in the T_2-weighted MR image (Fig. 7(b)). The average MR intensity in the tumor area, calculated from the MR image, decreased rapidly by 31.6% from 76.7±11.6 to 52.4±8.9, showing significant negative enhancement due to aggregation of the nanocapsules. In images taken from 1 h and 2 h after injection, the enhancement of the tumor was still clear, consistent with the MR intensity calculation. The images at 4 h and 24 h show no obvious change in contrast compared with the image at 2 h, suggesting the nanocapsules had been gradually cleared from the tumor and indicating that the nanocapsules can accumulate and remain in the tumor sites as long as two hours to provide adequate time for subsequent therapy. The accumulated nanocapsules also can display the tumor areas to guide the NIR laser irradiation for photothermal ablation of tumors without damaging the surrounding healthy tissues.

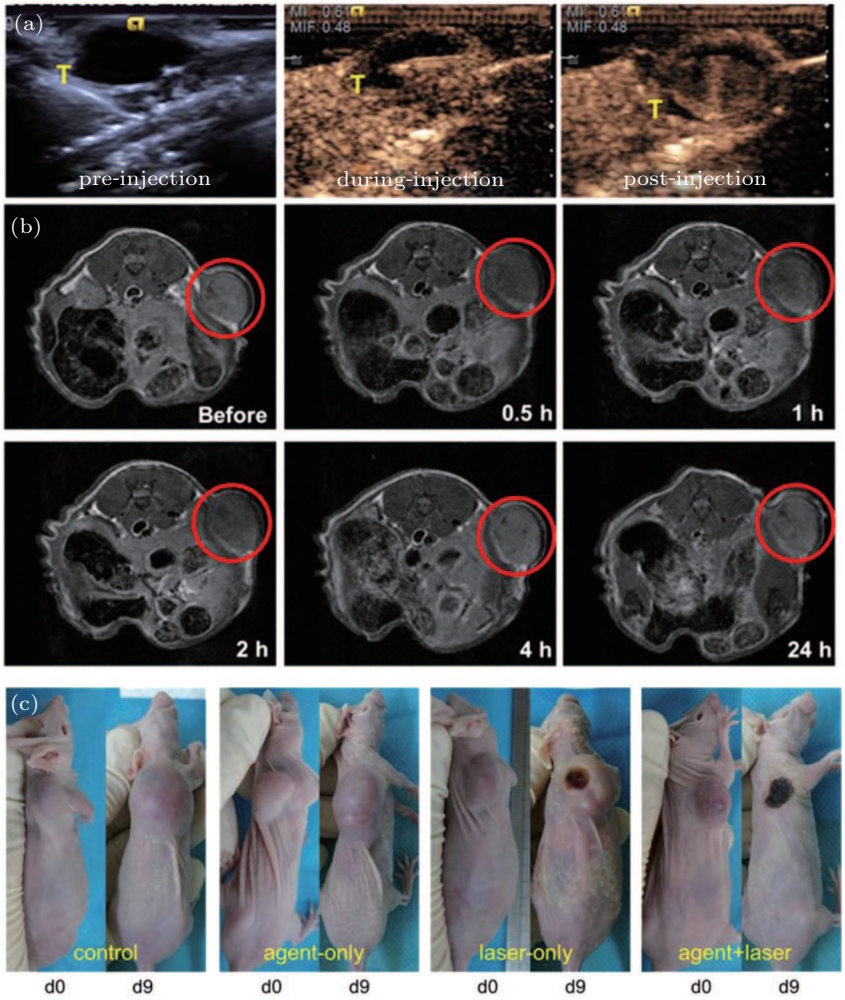


Fig. 7. (a) Contrast-enhanced ultrasonograms, before, during, and after the injection of the PGS-SP NCs (0.2 mL, 2 m·mL^{-1}) into the mice; (b) T_2-weighted MR images of the tumors at different time points after injection of the agent (0.15 mL, 2 mg·mL^{-1}); (c) Photographs of representative mice of the four different groups taken pre- and post-treatment.[58]

After intravenous injection of PGS-SP NCs into HT-1080 tumor-bearing nude mice followed by NIR laser irradiation, tumors decreased from 709±83.49 mm^3 to 444±227 mm^3 on the 9th day after treatment (34.0% smaller in tumor size). In comparison with control group (2499±230 mm^3 at day 9), the tumor growth was inhibited by 82.2%, suggesting that sufficient accumulation of PGS-SP NCs could trigger a great photothermal effect locally for effective photothermal tumor ablation. Furthermore, photographs of representative mice show that excellent therapeutic effectiveness was achieved by the combination of PGS-SP NCs with NIR laser irradiation (Fig. 7(c)). On the contrary, tumor growth was affected by either PGS-SP NCs or NIR laser irradiation alone. Therefore, effective photothermal tumor ablation was successfully carried out under the guidance of US/MRI contrast imaging due to the accumulation of nanocapsules in tumor sites through passive targeting.

5. Conclusion and perspectives

Theranostic magnetic NPs can provide contrast-enhanced and real-time images to guide an NIR laser to irradiate at the right location without damage to normal tissues, allowing the identification of the target site location and target-site distribution of pharmacologically active agents, as well as the prediction of treatment responses. The most noticeable feature of the platform is that all the procedures in the whole treatment are noninvasive or minimally invasive, avoiding unnecessary risk. MRI-guided photothermal therapy using multifunctional magnetic NPs enables "tailored treatment and facilitates (pre-) clinical efficacy and toxicity analyses, contributing substantially to realizing the potential of targeted therapeutic interventions. While the field has already seen great progress, exciting developments still lie ahead. We anticipate that magnetic theranostic agents will contribute to significant advances in the treatment of many classes of diseases. All these efforts will of course require interdisciplinary collaboration of chemists, materials scientists, biologists, pharmacologists, and physicians.

References

[1] Huang X, El-Sayed I H and Qian W 2006 *J. Am. Chem. Soc.* **128** 2115
[2] O'Neal D P, Hirsch L R and Halas N J 2004 *Cancer Lett.* **209** 171
[3] Rai P, Mallidi S and Zheng X 2010 *Adv. Drug Deliver. Rev.* **62** 1094
[4] Ke H T, Wang J R, Dai Z F, Jin Y S, Qu E Z, Xing Z W, Guo C X, Yue X L and Liu J B 2011 *Angew. Chem. Int. Ed.* **50** 3017
[5] Zha Z B, Zhang S H, Deng Z J, Li Y Y, Li C H and Dai Z F 2013 *Chem. Commun.* **49** 3455
[6] Zhang S H, Zha Z B, Yue X L, Liang X L and Dai Z F 2013 *Chem. Commun.* **49** 6776
[7] Jin Y S, Wang J R, Ke H T, Wang S M and Dai Z F 2013 *Biomaterials* **34** 4794
[8] Zha Z B, Deng Z J, Li Y Y, Li C H, Wang J R, Wang S M, Qu E Z and Dai Z F 2013 *Nanoscale* **5** 4462
[9] Zha Z B, Wang S M, Zhang S H, Qu E Z, Ke H T, Wang J R and Dai Z F 2013 *Nanoscale* **5** 3216
[10] Zha Z B, Yue X L, Ren Q S and Dai Z F 2013 *Adv. Mater.* **25** 777
[11] Liang X L, Li X D, Yue X L and Dai Z F 2011 *Angew. Chem. Int. Ed.* **50** 11622
[12] Ke H T, Wang J R, Dai Z F, Jin Y S, Qu E Z, Xing Z W, Guo C X and Yue X L 2011 *J. Mater. Chem.* **21** 5561
[13] Wang S M, Dai Z F, Ke H T, Qu E Z, Qi X X, Zhang K, Liu J B and Wang J R. 2013 *Eur. J. Radiol.* in press
[14] Zha Z B, Wang J R, Qu E Z, Zhang S H, Wang S M and Dai Z F 2013 *Sci. Rep.* in press
[15] Liang X L, Deng Z J, Jing L J, Li X D, Li C H, Huang M M and Dai Z F 2013 *Chem. Commun.* in press
[16] Fu G L, Liu W, Feng S S, Ma F and Yue X L 2012 *Chem. Commun.* **48** 11567
[17] Jing L J, Liang X L, Li X D, Yang Y B, Yue X L and Dai Z F 2013 *Acta Biomater*, in press
[18] Goldberg S N, Grassi C J and Cardella J F 2005 *Radiology* **235** 728
[19] Tran T D, Caruthers S D and Hughes M 2007 *Int. J. Nanomed.* **2** 515
[20] Louie A Y 2010 *Chem. Rev.* **110** 3146
[21] Gobin A M, Lee M H and Halas N J 2007 *Nano Lett.* **7** 1929
[22] Yoo D, Lee J H and Shin T H 2011 *Acc. Chem. Res.* **44** 863
[23] Tong S, Hou S and Zheng Z 2010 *Nano. Lett.* **10** 4607
[24] Laurent S, Forge D and Port M 2008 *Chem. Rev.* **108** 2064
[25] Ghosh D, Lee Y and Thomas S 2012 *Nat. Nanotechnol.* **7** 677
[26] Lee J H, Huh Y M and Jun Y W 2007 *Nat. Med.* **13** 95
[27] Zou P, Yu Y and Wang Y A 2010 *Mol. Pharm.* **7** 1974
[28] Yu Y and Sun D 2010 *Expert. Rev. Clin. Pharmacol.* **3** 117
[29] Raynal I, Prigent P and Peyramaure S 2004 *Invest. Radiol.* **39** 56
[30] Frangioni J V 2003 *Curr. Opin. Chem. Biol.* **7** 626
[31] Smith B A, Gammon S T, Xiao S Z, Wang W, Chapman S, McDermott R, Suckow M A, Johnson J R, Piwnica-Worms D, Gokel G W, Smith B D and Leevy W M 2011 *Mol. Pharm.* **8** 583
[32] Adams K E, Ke S, Kwon S, Liang F, Fan Z, Lu Y, Hirschi K, Mawad M E, Barry M A and Sevick-Muraca E M 2007 *J. Biomed. Opt.* **12** 0240171
[33] Desmettre T, Devoisselle J M and Mordon S 2000 *Surv. Ophthalmol.* **45** 15
[34] Maarek J M I, Holschneider D P and Harimoto J 2001 *J. Photochem. Photobiol. B* **65** 157
[35] Rudin M 2009 *Curr. Opin. Chem. Biol.* **13** 360
[36] Ma Y, Tong S, Bao G, Gao C and Dai Z F 2013 *Biomaterials* **34** 7706
[37] Makino A, Kizaka-Kondoh S, Yamahara R, Hara I, Kanzaki T, Ozeki E, Hiraoka M and Kimura S 2009 *Biomaterials* **30** 5156
[38] Rhyner M N, Smith A M, Gao X H, Mao H, Yang L L and Nie S M 2006 *Nanomedicine* **1** 209
[39] Needham D, Anyarambhatla G, Kong G and Dewhirst M W 2000 *Cancer Res.* **60** 1197
[40] Reimhult E, Amstad E A, Kohlbrecher E J, Muller E, Schweizer T and Textor M 2011 *Nano Lett.* **11** 1664
[41] Gao X H and Jin Y D 2009 *J. Am. Chem. Soc.* **131** 17774
[42] Dai Z F, Tian W J, Yue X L, Zheng Z Z, Qi J J, Tamai N and Kikuchi J 2009 *Chem. Commun.* **45** 2032
[43] Ma Y, Dai Z F, Gao Y G, Cao Z, Zha Z B, Yue X L and Kikuchi J 2011 *Nanotoxicology* **5** 622
[44] Jin Y S, Yue X L, Wu X Y, Cao Z and Dai Z F 2012 *Acta Biomater.* **8** 3372
[45] Liang X L, Yue X L, Dai Z F and Kikuch J 2011 *Chem. Commun.* **47** 4751
[46] Leung S L, Zha Z B, Teng W M, Cohn C, Dai Z F and Wu X Y 2012 *Soft Matter* **8** 5756
[47] Cao Z, Ma Y, Yue X L, Li S Z, Dai Z F and Kikuchi J 2010 *Chem. Commun.* **46** 5265
[48] Ma Y, Dai Z F, Zha Z B, Gao Y G and Yue X L 2011 *Biomaterials* **32** 9300
[49] Ma Y, Liang X L, Tong S, Bao G, Ren Q S and Dai Z F 2013 *Adv. Funct. Mater.* **23** 815
[50] Kinsella J M, Ananda S, Andrew J S, Grondek J F, Chien M P, Scadeng M, Gianneschi N C, Ruoslahti E and Sailor M J 2011 *Adv. Mater.* **23** H248.
[51] Ma L L, Feldman M D, Tam J M, Paranjape A S, Cheruku K K, Larson T A, Tam J O, Ingram D R, Paramita V, Villard J W, Jenkins J T, Wang T, Clarke G D, Asmis R, Sokolov K, Chandrasekar B, Milner T E and Johnston K P 2009 *Acs Nano* **3** 2686
[52] Cao Z, Yue X L, Li X D and Dai Z F 2013 *Langmuir* accepted
[53] Nikoobakht B and El-Sayed M A 2003 *Chem. Mater.* **15** 1957
[54] Xing Z W, Ke H T, Wang J R, Zhao B, Yue X L, Dai Z F and Liu J B 2010 *Nanotechnology* **21** 145607
[55] Xing Z W, Ke H T, Zhao B, Yue X L, Wang J R, Dai Z F and Liu J B 2010 *Acta Biomater.* **6** 3542
[56] Ke H T, Xing Z W, Zhao B, Wang J R, Liu J B, Guo C X, Yue X L, Liu S Q, Tang Z Y and Dai Z F 2009 *Nanotechnology* **20** 425105
[57] Yang F, Gu Z X, Jin X, Wang H Y and Gu N 2013 *Chin. Phys. B* **22** 104301
[58] Ke H T, Wang J R, Tong S, Jin Y S, Wang S M, Qu E Z, Bao G and Dai Z F 2013 *Theranostics* accepted.
[59] Reimer P and Balzer T 2003 *Eur. Radiol.* **13** 1266